Stacking Analysis of *Swift* GRBs

James Chiang[1] and Judith Racusin[2]
on behalf of the *Fermi* Large Area Telescope Collaboration
[1]KIPAC/SLAC
[2]NASA/GSFC

Summary: We stack the log-likelihood profiles from the source analyses of the *Swift* burst positions to look for evidence of extended emission. This stacking procedure enables us to increase our sensitivity by about an order-of-magnitude with respect to analysis of a single burst. We use the stacked estimates of the GeV flux to constrain the average SED of GRB afterglows on 10 ks time scales.

GeV Extended Emission

Late time emission (after the nominal prompt burst phase) has been detected routinely by the *Fermi* Large Area Telescope (LAT) in several LAT bursts, including the four brightest: GRB 080916C, GRB 090510, GRB 090902B, GRB 090926A (See Fig. 1). This "extended emission" exhibits a smooth temporal decay ($\sim t^{-1.2\text{–}1.7}$) and nearly constant power-law spectrum ($\sim E^{-2.1}$), in contrast to the strong temporal and spectral variability seen during the prompt phase. This suggests that the extended emission results from the external shock that produces the afterglow components at optical, UV, and X-ray wavelengths.

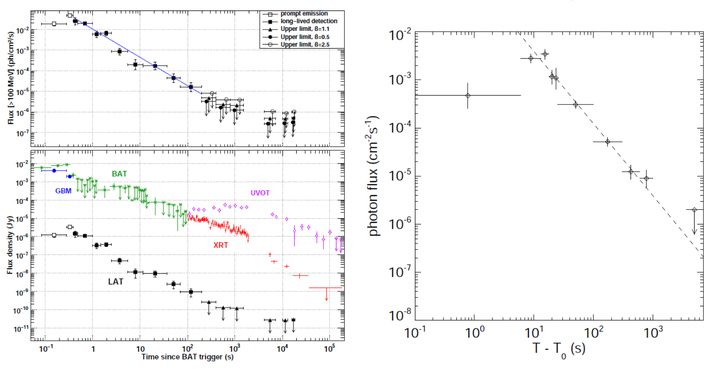

Figure 1: *Afterglow light curves for GRB 090510 (left, de Pasquale et al. 2009) and GRB 090902B (right, LAT only, Abdo et al. 2009)*

The *Swift* Sample

Even though most *Swift* GRBs occur outside of the LAT field-of-view (FoV) during the prompt phase, because of the LAT's survey rocking strategy, almost all *Swift* burst locations are observed by the LAT within 2 orbits. From Aug 2008 through Dec 2010, *Swift* BAT detected 157 bursts that also had an afterglow signal in the XRT. The LAT detected two with extended emission at high significance, GRB 090510 (de Pasquale et al. 2009) and GRB 100728A (Abdo et al. 2011). The remaining 155 bursts form the sample for our stacking analysis. The distributions of BAT T90 durations and fluences (15–150 keV, Sakamoto et al. 2011) are shown in Fig. 2.

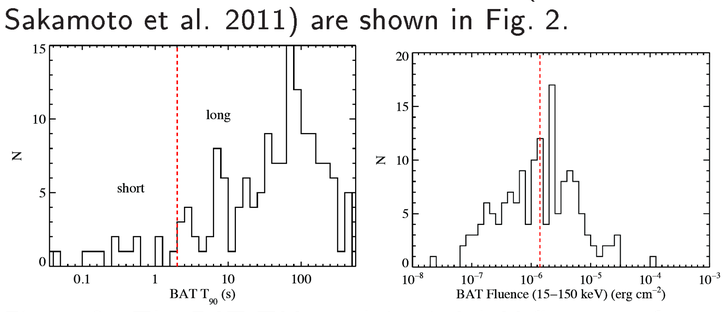

Figure 2: *The BAT T90s and 15–150 keV fluences of our sample. The vertical lines indicate the short vs long and low vs high fluence subsamples in the respective plots.*

Swift XRT Flux Calculations

- All X-ray afterglow light curves and spectral fits are from the Leicester XRT light curve repository (Evans et al. 2007, 2009).
- Flaring episodes are removed, and the light curves are fit with (broken) power-laws using methods of Racusin et al. (2009).
- X-ray fluxes during LAT intervals were averaged for comparison with the LAT fluxes.

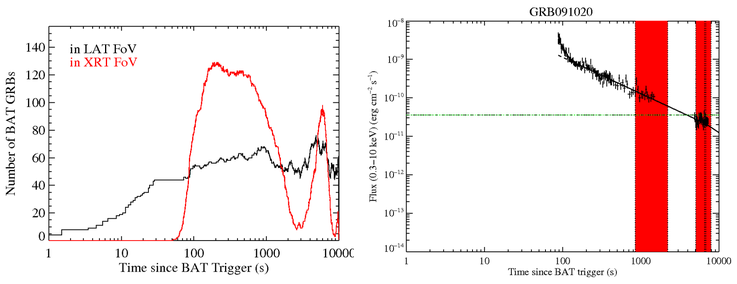

Figure 3: *Left: Number of BAT GRBs within the XRT and LAT FoVs as a function of time after the BAT trigger. Right: An example showing the overlap of X-ray flux measurements with LAT intervals (in red) used in computing the GeV emission.*

Stacking Results

The T_s profiles for the full 155 bursts over the 2 orbit interval (0–11.4 ks) after the BAT trigger are show in Fig. 4. Even though none of these profiles yields a significant detection, from the T_s profile, we can still infer the maximum likelihood estimates (MLEs) of the fluxes in the various bands: $F_{0.1-300} = 1.4^{+0.8}_{-0.6} \times 10^{-8}$ ph cm^{-2}s^{-1}, $F_{0.1-1} = 1.1^{+1.1}_{-0.9} \times 10^{-8}$ ph cm^{-2}s^{-1}, and $F_{1-300} = 3.3^{+2.2}_{-1.5} \times 10^{-9}$ ph cm^{-2}s^{-1} for the 0.1–300, 0.1–1, and 1–300 GeV bands, respectively. The latter two bands imply a photon spectral index of $\Gamma = 1.6 \pm 0.4$. This is somewhat harder than the value of 2.1 found for the bright LAT bursts but still within the 1-σ error.
Similar analyses for time intervals 0.1–1.14 ks and 1.14–11.4 ks yield fluxes of $F_{0.1-300} = 4.5^{+4.0}_{-2.8} \times 10^{-8}$ ph cm^{-2}s^{-1}and $F_{0.1-300} = 8.4^{+6.8}_{-5.2} \times 10^{-9}$ ph cm^{-2}s^{-1}, respectively. Although these measurements are even less significant than those for the full 0–11.4 ks interval, with $T_s = 3.6$ and 3.5, respectively, the fact that the flux in the earlier interval is substantially larger than that of the later one is consistent with the temporal decay of the extended emission seen in the bright LAT bursts. In fact, the fluxes in these two intervals imply a similar power-law temporal decay of $t^{-1.7\pm0.5}$

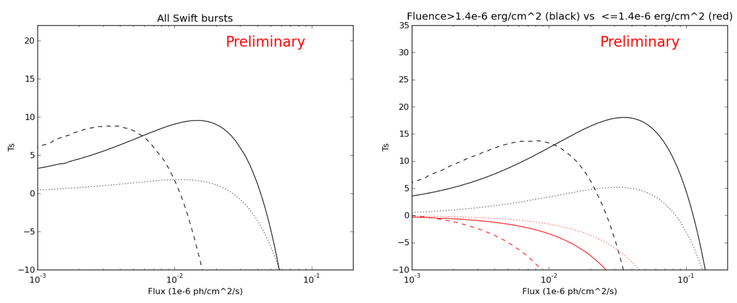

Figure 4: *Left: Stacked T_s profiles for the full 155 bursts sample over the 0–11.4 ks. The results are shown for the 0.1–300 GeV (solid curve), 0.1–1 GeV (dotted), and 1–300 GeV (dashed) data. Right: Results for two different subsamples: high (black curves) and low (red) BAT fluence bursts, as defined in Fig. 2.*

We have also considered various subselections of the data: long vs short duration, high vs low BAT fluence, UVOT-detection vs non-detection, and X-ray flares present vs no X-ray flares. Since these subselections may divide the sample in ways that are not necessarily related to the GeV properties, one doesn't want to consider too many different ex post alternatives. Nonetheless, among the four that we considered, we find a substantially increased significance for the high fluence subsample. For that subselection, the maximum profile value has $T_s = 18$ implying a flux of $F_{0.1-300} = 3.5^{+1.4}_{-1.2} \times 10^{-8}$ ph cm^{-2}s^{-1} (Fig. 4).

Afterglow SED

In Fig. 5, we show the "average" afterglow spectral energy distribution that we derive from the stacked LAT results and from the median and ±1-σ values of the XRT power-law spectra as a function of energy. Given the XRT curves, the LAT data points indicate an $\alpha_{X\gamma} \sim 1$ and suggest the existence of a synchrotron self-Compton component, assuming that the X-ray emission is synchrotron emission from an external shock. If the LAT data are SSC emission, the existence of such a component would have implications for the physical properties (e.g., particle density, size scale, etc.) of the emitting material. However, the need for an additional component depends on how the XRT spectra extrapolate to GeV energies. To give some indication of this, we also show in Fig. 5 the distribution of photon indices that were fit to the XRT data.

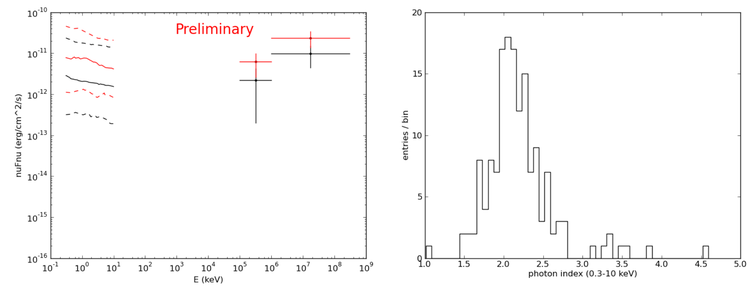

Figure 5: *Left: Afterglow SEDs for full 155 burst sample (black) and the 77 bursts in the high BAT fluence sample (red). For the XRT data, the solid curve is the sample median flux derived from the power-law fits and the dashed curves indicate the ±1-σ bounds. Right: Distribution of photon indices fit to the XRT data. The mean value of this distribution is $\Gamma_{\rm mean} = 2.19$ and the standard deviation is $\sigma_\Gamma = 0.44$.*

References

[1] Abdo, A. A., et al. 2009, ApJ, 706, L138.
[2] Abdo, A. A., et al. 2011, ApJ Letters, in press.
[3] de Pasquale et al. 2009, ApJ, 709, L146.
[4] Evans, P. A., et al. 2007, A&A, 469, 379.
[5] Evans, P. A., et al. 2009, MNRAS, 397, 1177.
[6] Racusin, J. L., et al. 2009, ApJ, 698, 43.
[7] Sakamoto, T., et al. 2011, arXiv:1104.4689.

LAT Stacking Procedure

The precise locations provided by *Swift* allow for an unbinned likelihood analysis of the LAT data. For each of the bursts, we perform the standard analysis:

- The source model for each consists of a point source at the Swift location + Galactic diffuse emission + isotropic diffuse component.
- Data is extracted in a 15° acceptance cone.
- The `P7SOURCE_V6` data selection and IRFs are used.
- Three energy bands: 0.1–300 GeV, 0.1–1 GeV, and 1–300 GeV. The latter two yield a photon index.
- We model the GRB spectrum as a power-law with a fixed photon index. Initially, the index is set to $\Gamma = 2.1$, the index found for the bright LAT bursts. We reanalyze using $\Gamma = 1.65$ for consistency with the value inferred from the 0.1–1 and 1–300 GeV bands.
- The profile likelihood is obtained by scanning in the flux parameter f, thereby yielding the best-fit flux and/or the 95% CL upper limit for each burst (Fig. 6).
- Formally, the "test statistic" T_s is defined as

$$T_s = 2(\log \mathcal{L}(f = 0) - \log \mathcal{L}(\hat{f})) \qquad (1)$$

where $\hat{f}$ is the MLE of the flux. For one degree-of-freedom, $\sqrt{T_s}$ corresponds to an $n\sigma$ detection. None of the 155 bursts has a $T_s > 9$.

- To find the MLE and confidence intervals of the stacked sample, we plot Eq. 1 as a function of the (non-MLE) values of f.

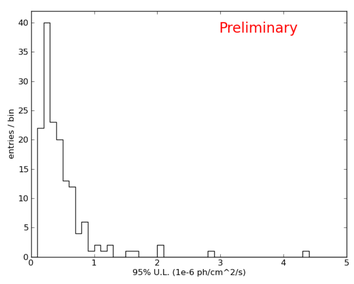

Figure 6: *Distribution of 95% confidence level upper limits for the 155* Swift *bursts in our stacking sample.*

To perform the stacking, we simply add the T_s profiles as a function of f. The peak of the resulting profile gives the stacked MLE of the population average flux. Note that the upper limits we find for the individual bursts peaks at $\sim$ few $\times 10^{-7}$ ph cm^{-2}s^{-1} and that the corresponding limit from Fig. 4 is about an order-of-magnitude lower, which is consistent with the expected $\mathcal{O}(N_{\rm samp}^{1/2})$ scaling.